

Environmental Science Nano

Accepted Manuscript



This is an *Accepted Manuscript*, which has been through the Royal Society of Chemistry peer review process and has been accepted for publication.

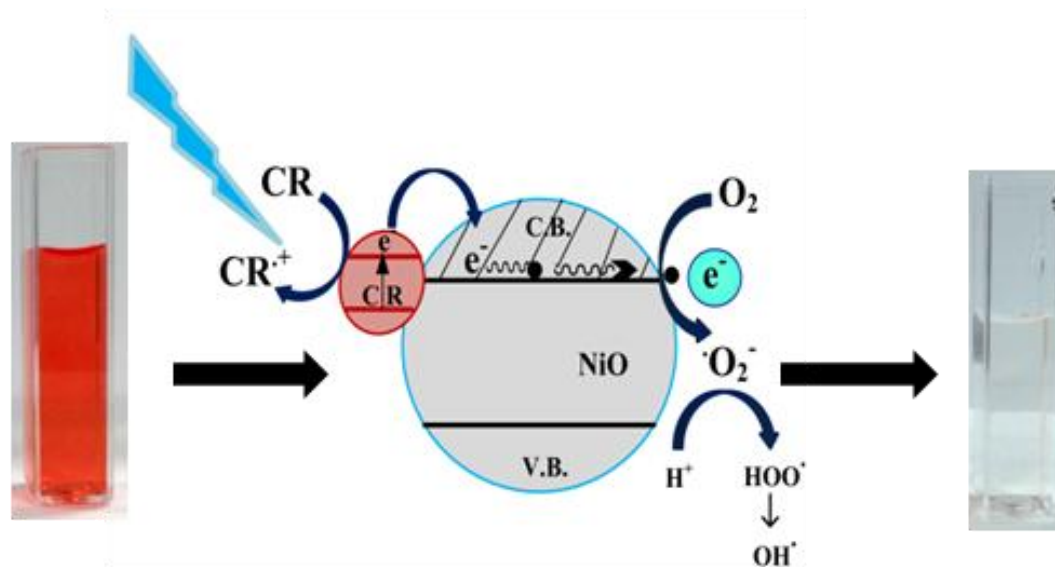
Accepted Manuscripts are published online shortly after acceptance, before technical editing, formatting and proof reading. Using this free service, authors can make their results available to the community, in citable form, before we publish the edited article. We will replace this *Accepted Manuscript* with the edited and formatted *Advance Article* as soon as it is available.

You can find more information about *Accepted Manuscripts* in the [Information for Authors](#).

Please note that technical editing may introduce minor changes to the text and/or graphics, which may alter content. The journal's standard [Terms & Conditions](#) and the [Ethical guidelines](#) still apply. In no event shall the Royal Society of Chemistry be held responsible for any errors or omissions in this *Accepted Manuscript* or any consequences arising from the use of any information it contains.

Nano impact

Metal oxide nanofibers present a better alternative in the waste water treatment as these are capable to degrade the organic wastes including hazardous dyes using advanced oxidation processes. Nickel oxide is one of the semiconductors which can be very well utilized in photocatalytic applications. With the huge utilization of dyes on the large scale, it is now required to come up with some new methodology that can treat these contaminants at low cost with greater efficiencies. This work is basically attributed to the economic degradation of congo red dye under the visible light irradiation where nickel oxide nanofibers were developed using versatile and cost effective electrospinning method. Development of such nanofibers for the degradation of highly stable azo dyes in the wastewater may act as a major component of nano-remediation process in the near future.

Graphical abstract

Cite this: DOI: 10.1039/c0xx00000x

www.rsc.org/xxxxxx

ARTICLE TYPE

Fabrication and characterization of poly (ethylene oxide) templated nickel oxide nanofibers for dye degradation

Deepika Malwal^a, P. Gopinath^{*a,b}

Received (in XXX, XXX) Xth XXXXXXXXXX 20XX, Accepted Xth XXXXXXXXXX 20XX

DOI: 10.1039/b000000x

In the present study, one dimensional nickel oxide (NiO) nanofibers were successfully fabricated using inexpensive and simplistic electrospinning technique to evaluate their efficient applicability as a photocatalyst in the dye degradation processes. The synthesis part involves the calcination of electrospun poly (ethylene oxide) /Nickel acetate tetrahydrate nanofibers to obtain phase pure cubic NiO nanofibers which were further characterized using various techniques for their physical and chemical properties. Furthermore, the photocatalytic activity of these NiO nanofibers along with their kinetics of degradation was studied with the photodegradation of model dye congo red (CR) under visible light irradiation. Interestingly, the photocatalytic properties of NiO nanofibers were found better than that of the nanoparticles when compared and found to be dependent on the concentrations of photocatalyst loaded. Besides this, the stability of the nanofibers in the aqueous solution was examined along with their reusability studies.

Introduction

In this 21st century, huge global industrialization has become a threat to the environment. Thousands of different dyes and pigments in millions of tons are being utilized annually worldwide not only in textile industries but also in various other industries like paper and pulp, plastics, cosmetics, leather industries and so on.¹⁻³ Besides this, most of the dyes used in the dyeing units are azo dyes containing chromophoric azo group (-N=N-) because of their wide range of bright shades, capability to bind with the fabrics strongly, ease of application and less energy consumption.⁴⁻⁵ Such widespread use of dyes, results in more discharge in the industrial effluents, presenting a great hazard for all living beings of the ecosystem ranging from aquatic organisms to human beings. Basically, the dyes present in water reduce the photosynthetic activity of aquatic plants by interrupting the incoming sunrays and gas dissolution resulting in the destruction of aquatic ecosystem.⁶ Moreover, most of the dyes are carcinogenic and mutagenic in nature responsible for various types of cancer.⁷

CR is a benzidine based diazo dye (Fig. 1), commonly used in the textile industries as well as in molecular biology laboratories for staining purposes because of its high water solubility, bright red colour with yellow fluorescence and high affinity of interaction with the fabrics. But it is highly toxic as its main component benzidine is known as human carcinogen and it is very difficult to degrade such kinds of dyes using conventional methodologies.⁸ Although various waste water treating chemicals, such as alum, activated carbon, ferric chloride (FeCl₃), CaCl₂ modified bentonite etc., are available but these are expensive and do not reduce the toxicity of dyes as well.⁹⁻¹⁰ To overcome these problems, semiconductors present a good option

for the photocatalysis of organic pollutants like dyes utilizing visible light and the oxygen present in air creating reactive oxygen species.¹¹

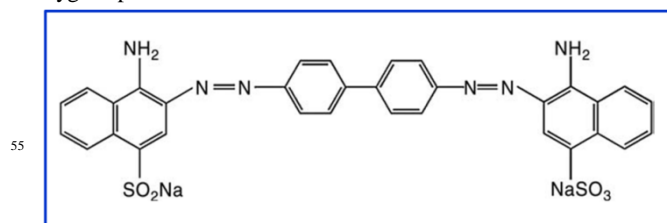


Fig. 1 Molecular structure of congo red (CR) dye

For the last some years, nanotechnology has contributed in diverse fields of research. A wide range of metal oxide nanostructures have been extensively explored in the field of photocatalysis out of which, nanoparticles are the most commonly exploited due to their highest surface area and hence high catalytic activity. However, these nanoparticles tend to agglomerate in the aqueous solution during the dye degradation process which subsequently reduces the catalytic activity of these nanoparticles.¹² To eradicate this problem of agglomeration and thus to improve the photocatalytic activity, one dimensional nanostructures are being synthesized, such as nanowires, nanotubes, nanofibers etc. Therefore metal oxide nanofibers are highly desirable and a topic of extensive research in the decoloration and degradation experiments because of their high surface area, better chemical stability, increased shelf life and higher porosity.^{13, 14} Among various metal oxides, nickel oxide with a wide band gap (3.7-4.0) is widely utilized in photocatalysis, electrochromic materials, electrode material for

lithium-ion batteries, magnetic high storage devices, sensors etc.¹⁵⁻¹⁸ Here we are going to explore the photocatalytic activity of nickel oxide nanofibers. But, its industrial application requires a worthwhile process to fabricate nanofibers. Amongst various other intricate methodologies, electrospinning is a simplistic and reliable technique to draw very fine continuous nanofibers from the polymeric solution, polymeric blends or sol-gel under high voltage making this remediation process highly cost effective at large scale.¹⁹

10 Results and Discussion

A wide range of materials have been exploited for the fabrication of ultrathin and smooth nanofibers using well known and versatile electrospinning technique. In the formation of continuous metal nanofibers, polymer plays an important role.²⁰ Various polymers are utilized as “carrier polymers” in the synthesis of composite nanofibers but it is preferred to use high molecular weight polymer that not only makes the final blend electrospinnable but also enables us to increase the concentration of main component in greater quantity.^{22,23} Polyethylene oxide (PEO) is such a high molecular weight polymer which was used as a carrier matrix for the synthesis of NiO nanofibers. Moreover, it is water soluble that avoids the use of organic solvents making the process cost-effective. Nickel oxide (NiO) nanofibers were obtained by coupling the electrospinning technique with subsequent calcination at 500°C. The whole fabrication procedure is presented in the scheme S1. Nickel acetate (NiAc) solution alone cannot be electrospun because it needs certain viscosity to draw the fibers. Therefore, PEO was utilized as a carrier in the formation of NiO nanofibers.

The parameters such as, viscosity, flow rate, distance between the needle and the collector, calcination temperature and duration etc. were optimized to get very fine and continuous nickel oxide nanofibers. The morphology of the fibers was confirmed by field emission scanning electron microscopy (FE-SEM) analysis. Fig. 2(a) represents FE-SEM image of NiAc/PEO composite nanofibers generated from 4.5 wt % PEO and 20 wt % nickel acetate. The obtained nanofibers were uniform, round and smooth with a mean diameter of 202.72 ± 20.72 nm as shown in the diameter distribution histogram (inset in Fig. 2(a)). The morphology of the nanofibers was found to be greatly affected by flow rate as high flow rate led to the formation of beads and less flow rate did not result in the formation of fiber because polymer got dried at the tip of needle and choked the extrusion of polymer from the needle. Therefore an intermediate flow rate i.e. 0.25 mL/h was opted to draw ultrathin nanofibers. The as-prepared nanofibers were further calcined at 500°C for 4 hours in the presence of air to obtain pure NiO nanofibers as represented in Fig. 2(b). After calcination, nanofibers became rough and a huge reduction in the size was observed; the mean diameter of the calcined NiO nanofibers was 57.17 ± 8.52 nm (inset in Fig. 2(b)). This is due to the fact that at such a high temperature, the entire polymer gets decomposed and conversion of NiAc into NiO takes place. This result was further confirmed by energy dispersive x-ray spectroscopy (EDX) analysis (Fig. S2) representing the elemental composition of NiO nanofibers assuring the presence of nickel and oxygen with the absence of polymer.

NiO nanoparticles were synthesised to compare the efficiency

of NiO nanofibers with NiO nanoparticles. Further the NiO nanofibers and nanoparticles were examined for their cross sectional information using transmission electron microscopy (TEM). Fig. 3(a) and 3(b) represents the TEM images of the calcined nanofibers at different magnifications confirming its size in the range of 50-60 nm. Along with this, selected area electron diffraction (SAED) pattern (inset in Fig. 3(a)) depicts the polycrystalline nature of the NiO nanofibers as obvious rings can be easily seen. The transmission electron micrograph of NiO nanoparticles (Fig. 3(c)) indicates the uniform size distribution of the particles. The mean diameter of the nanoparticles was found to be 23.167 ± 3.37 nm as shown in the particle diameter distribution histogram (Fig. 3d). Clear spots observed in the SAED pattern (inset in Fig. 3 (c)) further explain the crystalline nature of the NiO nanoparticles.

The crystalline structure of nanofibers and nanoparticles were further analyzed by X-ray diffraction (XRD). Fig. 4(a) elucidates the typical XRD pattern of NiO nanofibers and nanoparticles where the standard

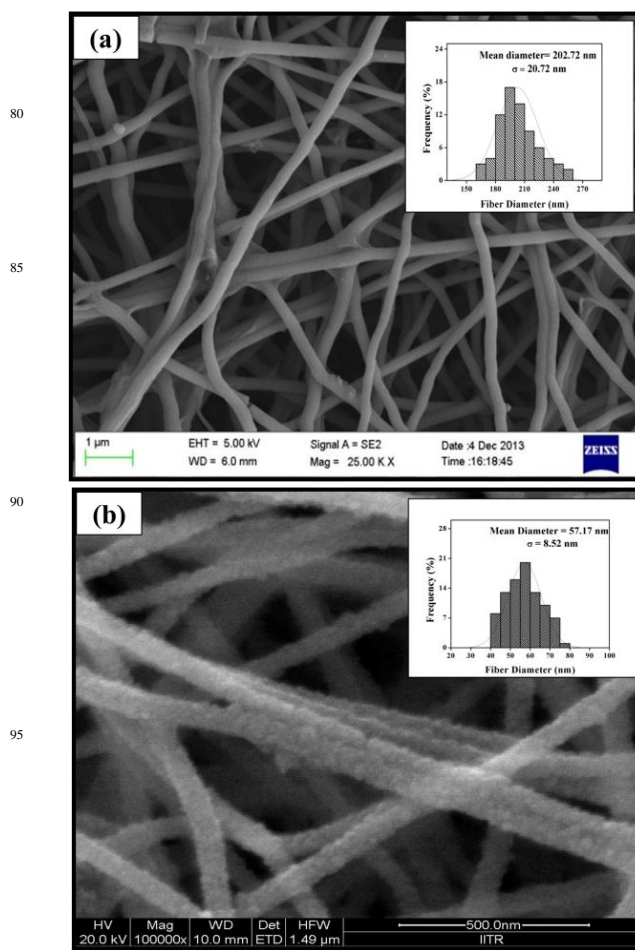


Fig. 2 FE-SEM images of (a) PEO/ Nickel acetate nanofibers (b) NiO nanofibers obtained after calcination at 500°C. The insets represent the diameter distribution histogram for the respective image.

peaks of NiO were observed. In case of nanofibers, very sharp and intense diffraction peaks were obtained at 2θ value of 37.21, 43.29, 62.88, 75.44 and 79.36° corresponding to (111), (200), (220), (311) and (222) crystal planes, respectively according to

JCPDS card number 01-071-1179. It indicates the formation of phase pure cubic NiO with rock salt structure (Bunsenite, NaCl type structure). In the XRD pattern of NiO nanoparticles, very sharp diffraction peaks at 2θ value of 37.34, 43.40, 63.02, 75.51 and 79.52° were perfectly indexed as (111), (200), (220), (311) and (222) planes, respectively according to the JCPDS card number 01-073-1519 which strongly determines the cubic crystalline nature of the nanoparticles. The crystallite size of the particle was also calculated using the Scherrer formula ($t = K\lambda/B\cos\theta$) where t is the crystallite size, K is the constant having value 0.9, λ is wavelength of Cu $K\alpha$ radiation which is equal to 0.154 nm, B is full width at half maximum (FWHM). Using this formula, the crystallite size was found to be 25.6 nm which is in accordance with the size calculated from the diameter distribution histogram. Besides this, Fig. 4(b) represents the

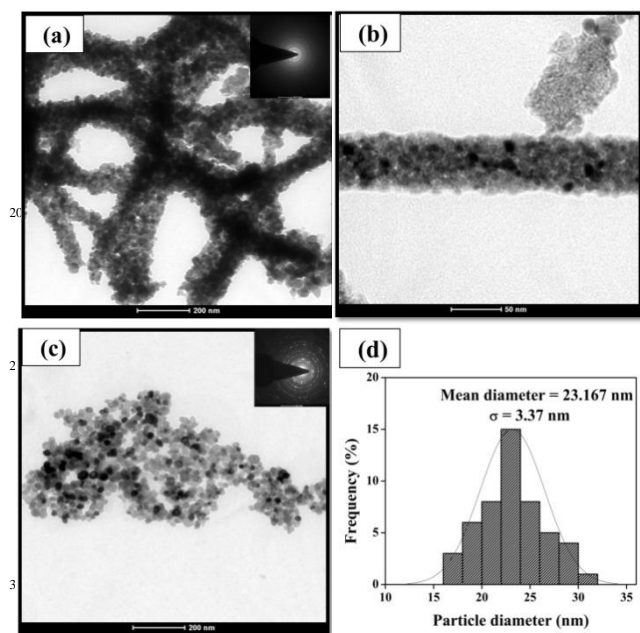


Fig. 3 TEM images of (a), (b) calcined NiO nanofibers at different magnifications along with the SAED pattern in the inset, (c) NiO nanoparticles with its SAED pattern (inset); (d) size distribution histogram for NiO nanoparticles demonstrating the mean diameter 23.167 nm with standard deviation 3.37 nm.

typical XRD pattern for pure PEO where two diffraction peaks were observed at 19.3 and 23.4° indicating (120) and (112) planes, respectively. Xu et al., detailed about the crystalline structure of pure PEO in which PEO shows a monoclinic crystalline structure where (120) planes lies parallel to the PEO chain direction and (112) planes intersect the chain direction.²⁴

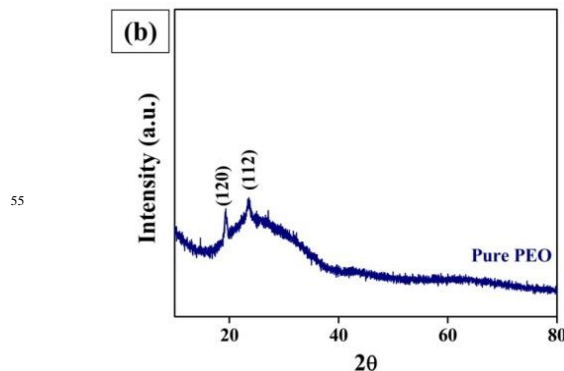
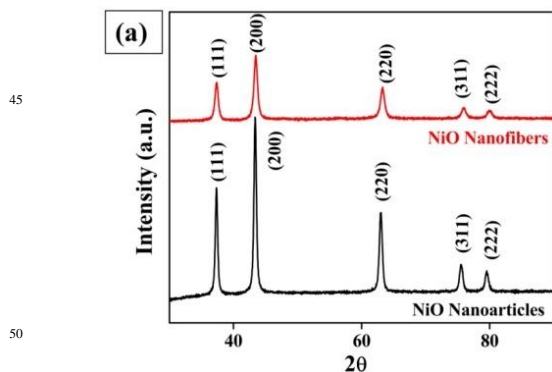


Fig. 4 XRD pattern for (a) NiO nanoparticles and nanofibers (b) pure PEO nanofibers.

In addition to this, when XRD patterns of nanofibers made up of PEO alone and that of NiO were compared, it was observed that the peaks due to the polymer completely disappeared after the calcination of nanofibers indicating the formation of phase pure NiO.

The formation of NiO from nickel acetate tetrahydrate can be evaluated by recording the chemical changes occurring in the sample with a constant heating rate.²⁵ Fig. 5 represents the stepwise decomposition of NiAc/PEO composite nanofibers and PEO alone nanofibers during constant heating in the presence of air up to 600°C. As temperature increased, weight started to decrease more rapidly for NiAc/PEO nanofibers as compared to that of PEO alone. The thermogram of pure PEO nanofibers shows the three steps decomposition. It was observed that PEO was stable up to 150°C and small weight loss occurs at 165°C which is due to presence of moisture attached with the nanofibers. After that, rapid degradation was observed leading to the complete decomposition at 333°C. In case of NiAc/PEO nanofibers, weight loss starts at near 50°C with the liberation of physical water content (e.g. moisture). With the constant increase in temperature, the water molecules attached with the nickel acetate molecules get released resulting in the complete dehydration of the sample. In the range of 127-273°C, the peaks observed are due to the decomposition of the organic matter like acetate groups and polymer. Beyond 273°C, no significant weight loss was observed which indicates the presence of only inorganic contents. According to the protocol followed for synthesis of nanofibers, calcination of the NiAc/PEO nanofibers was performed at 500°C, which suggests the complete decomposition of the polymer along with the formation of NiO and thus compliment well with all other characterization data.

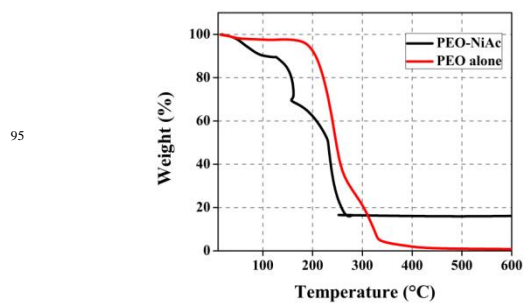


Fig. 5 TGA spectra for PEO/NiAc and PEO alone nanofibers indicating the chemical changes occurring in the fibers during the formation of NiO from nickel acetate/PEO.

Photodegradation of CR dye using NiO nanofibers

In the past, photocatalytic properties of various metal oxides have been extensively studied where possible mechanisms of action have been reported. When 6 mg NiO nanofibers were added to 60 ppm CR aqueous solution, most of the dye was degraded within a time period of 6 hours. The constant reduction in the concentration of dye was observed by taking absorbance at 500 nm using UV-Visible spectrophotometer which exploits the well known Beer Lambert's law (Fig. 6 (a)). The concentration of the dye can be calculated by plotting a calibration curve between different concentrations of dye vs their corresponding absorbance (Fig. S1). Additionally, control experiment was also performed with nanofibers in the dark conditions. Negligible degradation or decolorization was observed in the absence of light indicating the requirement of light for the effective decomposition of dye molecules. The plot depicting the degradation efficiency was constructed between the percentage of dye left ($A/A_0 \times 100$) versus time (hours) as shown in Fig. 6 (c) where A is the absorbance of dye at a particular time and A_0 is the absorbance obtained by initial concentration of dye. In this study, it is clearly evident that after 15 minutes, about 50 % dye was degraded and within 6 hours 98 % dye was degraded.

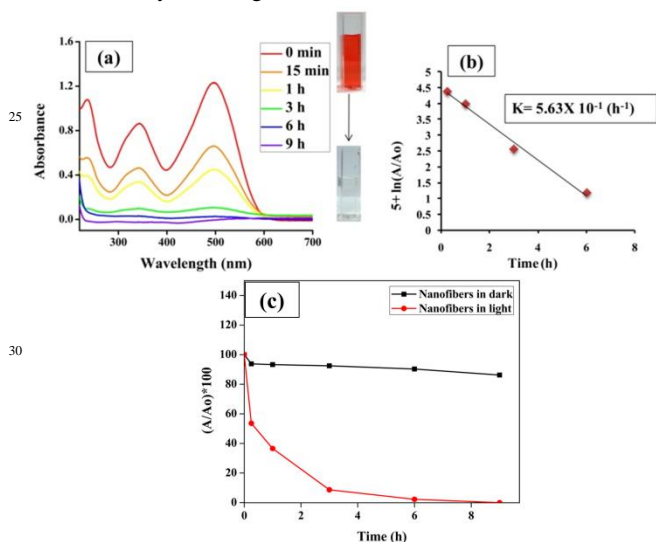
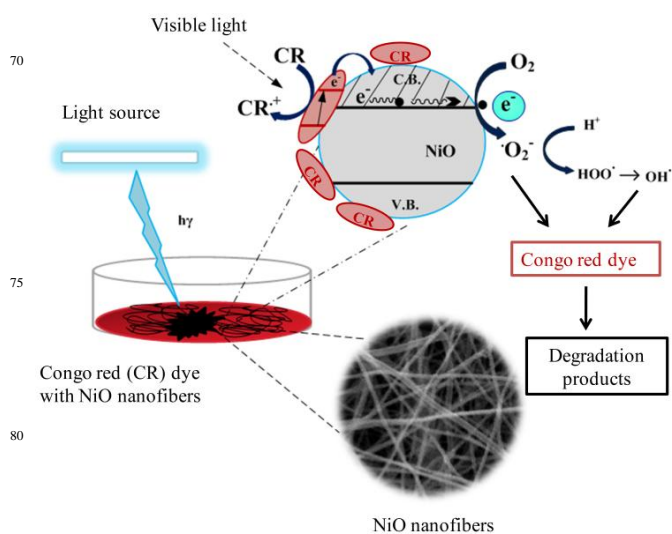


Fig. 6 (a) UV-Vis spectra representing reduction in concentration of CR dye along with decoloration of dye from dark red to clear solution as shown in inset (b) rate constant calculated for dye degradation reaction following pseudo first order reaction (c) Degradation efficiency of nanofibers in degradation of dyes in light and dark conditions.

The possible catalytic action of NiO for the degradation of dyes is same as that of other metal oxide semiconductors^{26,27} which is represented schematically in the scheme 1. In the present study, visible light was utilized for the CR degradation experiment but visible light does not possess sufficient energy to excite the electrons from valence band to conduction band of NiO. Therefore, a different mechanism is opted by the catalyst to degrade the dye which is known as photosensitized oxidation where CR molecules adsorb onto the surface of NiO catalyst and act as light harvesting molecules. Visible light excites the dye molecules (CR) rather than the catalyst adsorbed onto the photocatalyst and directly injects excited electron into the

conduction band of the photocatalyst in the time scale of nanosecond, whereas back transfer of electrons from CB to dye molecules is much slower. Thus, probability of electron transfer from CB to surface of catalyst and the oxidized dye to react increases. In turn, the surface electrons react with the ambient oxygen (O_2) to create highly reactive oxygen species whereas sensitized dye gets converted into cationic dye radicals (equations 1-3).^{28,29} The superoxide anions subsequently get protonated to generate $HOO\cdot$ (free radicals) as shown in equation 4; which further react to produce hydroxyl radicals ($OH\cdot$) (equation 4-6). Thus generated hydroxyl free radicals ($OH\cdot$) attack the benzene ring directly linked to the azo bond resulting in the opening of the aromatic ring and hence generates CO_2 , H_2O and small organic acid molecules.³⁰⁻³² The color of the azo dyes is due to this azo group only and breakdown of this bond enables us to visualize the degradation of dyes³³. This oxidative degradation is consistent with the FTIR analysis.



Scheme 1 Proposed mechanism of action of NiO nanofibers for the photodegradation of congo red (CR) dye aqueous solution.

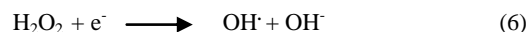
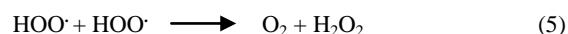
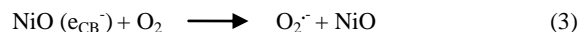
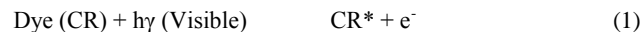


Fig. 7 illustrates the FTIR spectra of NiO nanofibers and the CR solution before and after the treatment with NiO nanofibers and nanoparticles. FTIR is usually used to reveal the chemical structure and the functional groups. In Fig 7(a), a prominent peak can be observed which is due to the Ni-O stretching vibrations along with the peaks at 1121, 1403, 1587 and 1627 cm^{-1} corresponding to C-N stretch, C-C bond, C-C bond and N-H bend, respectively. Fig. 7 (b) further depicts the spectra for CR

dye before treatment. The absorption peaks at 1633, 1586, 1404 and 1044 cm^{-1} were attributed to the N-H bend of primary amine, azo group (-N=N-), C-C stretch in aromatic rings (aromatic skeletal vibrations) and S=O stretch, respectively.

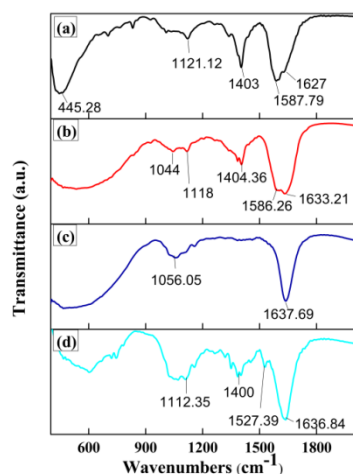


Fig. 7 FTIR spectra for (a) NiO nanofibers (b) CR before treatment (c) CR treated with nanofibers (d) CR treated with nanoparticles.

Treatment of aqueous congo red solution using nanofibers and nanoparticles causes a large number of changes in the chemical structure which is evaluated using these spectra (Fig. 7 (c) and (d)). In case of nanofibers, peaks due to azo group and C-C bonds in aromatic rings disappear completely indicating the cleavage of these bonds. In contrast to this, many peaks could be observed in case of nanoparticles. A significant peak at 1400 cm^{-1} attributed to C-C bond (aromatic ring) is observed which also indicates the better catalytic efficiency of NiO nanofibers as compared to NiO nanoparticles.^{34,35}

In context to the by-products of CR, FTIR provides lots of useful information. Degradation of CR dye initiates with the cleavage of the azo bond resulting in the generation of aromatic intermediates like aromatic amines or phenolic compounds. After that, the aromatic and naphthalene rings open up to form several organic acids like formic acid, acetic acid, oxalic acid etc. In the most dye degradation process, formic acid and acetic acid are produced.³⁶ Many of these intermediates may finally get decomposed into CO_2 , NH_4^+ , NO_3^- and SO_4^{2-} . The generation of these by-products can be correlated with the FTIR spectra (Fig. 7) provided in the manuscript. In Fig. 7 (c) There are absorption peaks at 1637 and 1156 cm^{-1} corresponding to the amine group (N-H) and sulphate group (S—O stretch), respectively depicting the presence of the NH_4^+ and SO_4^{2-} . Though from the FTIR results, this could be the most probable mechanism of dye degradation, other alternative mechanism cannot be excluded on the basis of FTIR.

Further, the kinetics of the photocatalytic degradation of CR was studied and it was observed that the degradation process follows pseudo first order reaction as straight lines were obtained in the plot (Fig. 6 (b)) constructed between $\ln(A/A_0)$ versus time (h). The rate constant (k) for the reaction can be calculated either by the slope of the graph or using the following kinetic equation:

$$\ln(A/A_0) = -kt$$

where A_0 and A represents absorbance for the initial concentration of dye (0 min) and at a particular time, respectively. The calculated rate constant k (h^{-1}) for this photodegradation reaction was found to be 0.563.

Moreover, amount of nanofibers to be added plays very important role in dye removal. As the amount of NiO nanofibers loaded increases, time of degradation decreases as more number of hydroxyl free radicals will be produced and action of degradation will become fast. It was observed that within 9 hours 60 ppm dye was completely degraded with 6 mg nanofibers where with 2 mg nanofibers 17 % dye was still there in the solution after 9 h. Fig. 8(a) represents the time dependent graphs for the dye degraded with 2 mg, 4 mg and 6 mg. Fig. 8(b) is the graph constructed to calculate the rate constants for three different concentrations of nanofibers used in the study. The rate constant for 2 mg concentration was observed to be the least and highest for the 6 mg nanofibers. All the rate constants have been represented in tabular form (Table S1) indicating that the rate constant is increasing with the amount of loading.

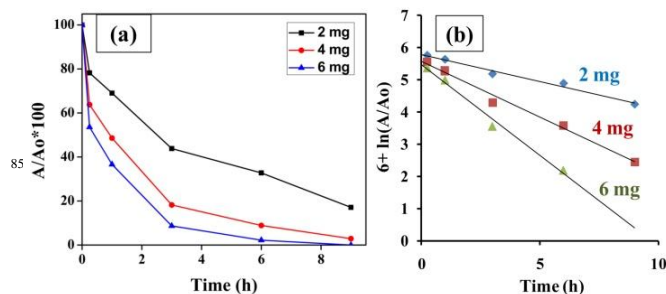


Fig. 8 (a) Concentration dependent studies utilizing 2 mg, 4 mg and 6 mg NiO nanofibers for same concentration of dye (60 ppm) (b) Rate constants evaluated for the photodegradation reactions with different loadings of nanofibers.

Comparative studies of NiO nanofibers and nanoparticles

NiO nanoparticles have been widely utilized as photocatalysts but limit their applicability in dye degradation and other waste water treatments processes due to their tendency to get aggregated in the aqueous solution. The fibers remain intact throughout the degradation process which enables better recovery of NiO nanofibers as compared to NiO nanoparticles after the treatment process. It extends its scope for reusability which may be difficult in case of nanoparticles as they are well dispersed in the aqueous solution and hence difficult to recover. Therefore the cost of treatment process would be drastically reduced as NiO nanofibers can be reused for multiple cycles and also because it does not require downstream processing of water for NiO contamination.³⁶ Furthermore, efficacies of both nanofibers and nanoparticles were examined practically by comparing the photocatalytic activity of NiO nanofibers and NiO nanoparticles. The reduction in the dye concentration was analyzed spectrophotometrically as Fig. 9(a) and 9(b) represents the UV-Vis spectra for the CR degradation using NiO nanofibers and nanoparticles, respectively. Same amount of nanofibers and

nanoparticles were loaded in the same concentration of dye under similar experimental conditions. By noting down the absorbance at 500 nm, a comparative plot was constructed (Fig. 9(c)) depicting the better photocatalytic activity of nanofibers as compared to the nanoparticles. It was observed that within 8 hours of treatment, 70% dye was degraded by nanofibers while 50% dye was still left in case of nanoparticles. Although a small reduction in the dye concentration was observed in the dye alone due to the presence of light but it was not significant. Followed by this, rate constants were calculated (Fig. 9(d)) for the photodegradation processes deploying the nanofibers and nanoparticles and were found to be 6.7×10^{-2} and 3.7×10^{-2} (h^{-1}), respectively. It was observed that rate constant for the reaction involving nanofibers was higher than that of the nanoparticles indicating the better degradation capability. Both the photocatalysts follow the pseudo first order reaction for their action.

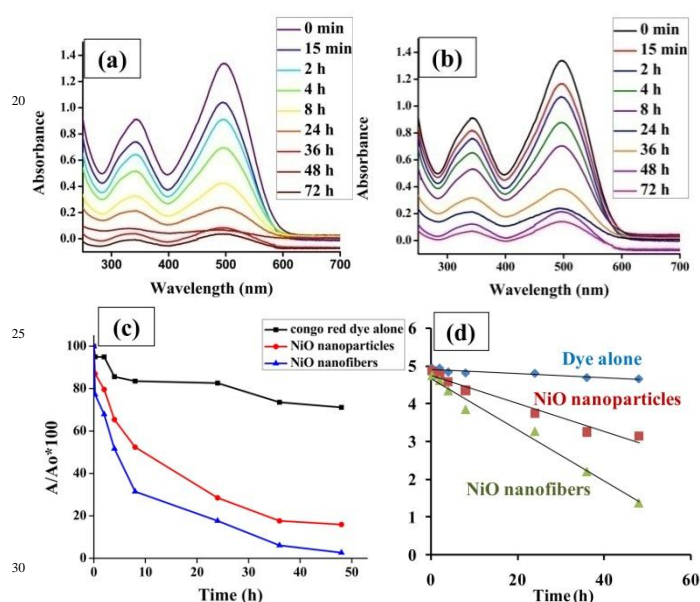


Fig. 9 UV-Vis spectra of CR dye degradation using (a) NiO nanofibers, (b) NiO nanoparticles; (c) comparative plot of NiO nanofibers and nanoparticles along with the CR dye alone; (d) rate constants for nanoparticles and nanofibers.

Reusability studies of NiO nanofibers

Stability and reusability is a serious issue while developing any photocatalyst for the waste water treatment as it will affect the cost of the treatment process. It is highly desirable that the photocatalyst should be stable enough so that it can be reused for long time enhancing the practical utility of these fibers. It could be concluded from Fig. 10(a) that NiO nanofibers can be reused as same nanofibers were used for three subsequent batches of CR aqueous solution. The result depicts a slight decrease in the degradation efficiency after first cycle. It may be due to the loss of the catalyst during washing and filtration so as to use in the next cycle.³⁸ The other important reason behind this large drop may be the poisoning of the catalyst. Some of the intermediate products remain attached over the surface of the nanofibers which hinder the adherence of other dye molecules and hence the degradation efficiency reduces with each cycle. Besides this,

stability of the nanofibers was investigated using FE-SEM analysis. No morphological changes were found in the NiO nanofibers after three cycles of reaction indicating the high stability of the photocatalyst (Fig. 10 (b)).

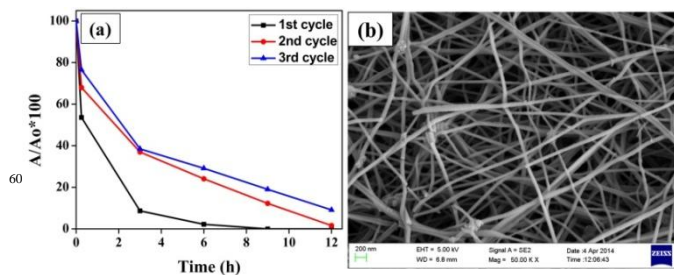


Fig. 10 (a) Plot representing the dye degradation efficiency of the NiO nanofibers for subsequent three batches of congo red aqueous solution (b) FE-SEM image of the used NiO nanofibers depicting no morphological changes even after three cycles of reaction.

Effect of pH on the stability of the nanofibers was also investigated. Fig. 11 represents the FE-SEM images of the used fibers in the treatment of aqueous dye solution having different pH values ranging from highly acidic (pH=3) to highly alkaline (pH=11). Interestingly, no morphological change was observed, except at extremely acidic conditions (pH=3), clearly demonstrating the stability of nanofibers.

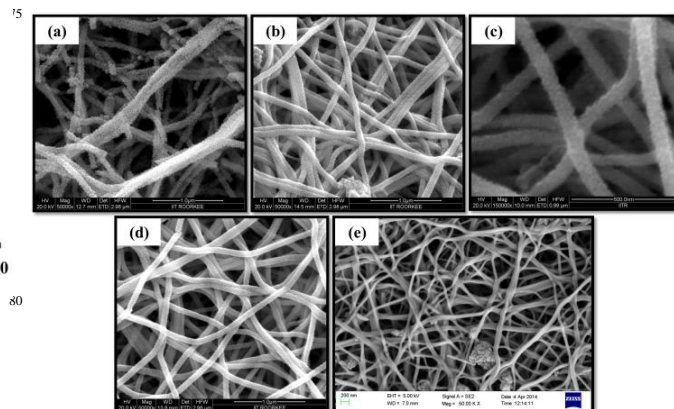


Fig. 11 FE-SEM images of NiO nanofibers after treatment of CR solution having pH (a) 3, (b) 5, (c) 7, (d) 9 and (e) 11.

Release of Ni during the treatment

Since high concentration of nickel is toxic for the humans as well as aquatic lives, release of nickel in the water during the treatment has to be examined. The concentration of Ni leached in the treated water using NiO nanofibers was observed to be 23.16 $\mu\text{g/L}$ which was much lower. This release of Ni further depends upon the pH of the contaminated water (Table S2). An experiment was conducted with 5 different CR aqueous solution having pH 3, 5, 7, 9 and 11. After the treatment, very low concentration of nickel was noted in all the samples except under extremely acidic conditions (pH=3). This faster rate of dissolution observed was due to attack of acid on the fibers.

Conclusion

In summary, we have synthesized highly stable and ultrafine NiO nanofibers using very cost-effective electrospinning technique. These NiO nanofibers act as an efficient photocatalyst in dye degradation processes generally required in dyeing units of various industries. All the characterization results confirm the synthesis of continuous, cubic NiO nanofibers and nanoparticles with mean diameter of 57.17 nm and 23.17 nm, respectively. The NiO nanofibers were observed as efficient photocatalyst capable to degrade the CR dye following the pseudo first order reaction. The concentration of catalyst to be used has significant effect on the dye degradation experiments as more the amount of nanofibers will be added, more rapidly the dye will get degraded. Also, NiO nanofibers were found to be better photocatalyst than NiO nanoparticles because of their non-aggregating nature in aqueous solution. In addition to this, reusability and stability are other advantages of these nanofibers without losing much of its efficacy in subsequent cycles of dye degradation reactions. Thus development of such nanofibers by electrospinning represents a very simple and cost effective approach for the degradation of highly stable azo dyes in the wastewater and it may act as a major component of nano-remediation process in the near future.

Notes and references

^a Nanobiotechnology Laboratory, Centre for Nanotechnology,

^b Department of Biotechnology,

Indian Institute of Technology Roorkee, Roorkee, Uttarakhand-247667, India. Fax: +91-1332-273560; Tel: 91-1332-285650; E-mail: pgopifnt@iitr.ernet.in, genegopi@gmail.com

† Electronic Supplementary Information (ESI) available: [details of any supplementary information available should be included here]. See DOI: 10.1039/b000000x/

1. G. Mezohegyi, A. Fabregat, J. Font, C. Bengoa, F. Stuber, *Ind. Eng. Chem. Res.*, 2009, **48**, 7054.
2. U. G. Akpan, B. H. Hameed, *J. Hazard. Mater.*, 2009, **170**, 520.
3. H. M. Pinheiro, E. Touraud, O. Thomas, *Dyes Pigm.*, 2004, **61**, 121.
4. L. Hua, H. Ma, L. Zhang, *Chemosphere*, 2013, **90**, 143
5. M. A. Rauf, M. A. Meetani, S. Hisaindee, *Desalination*, 2011, **276**, 13.
6. S. Zhu, S. Jiao, Z. Liu, G. Pang, S. Feng, *Environ. Sci.: Nano*, 2014, **1**, 172.
7. N. Puvaneswari, J. Muthukrishnan, P. Gunasekaran, *Indian J. Exp. Biol.*, 2006, **44**, 618.
8. A. Mittal, J. Mittal, A. Malviya, V. K. Gupta, *J. Colloid Interface Sci.*, 2009, **340**, 16.
9. N. Kannan, M. Meenakshisundaram, *Water Air Soil Pollut.*, 2002, **138**, 289.
10. P. M. K. Reddy, S. Mahammadunnisa, B. Ramaraju, B. Sreedhar, C. Subrahmanyam, *Environ. Sci. Pollut. Res.*, 2013, **20**, 4111.
11. C. Chen, W. Ma, J. Zhao, *Chem. Soc. Rev.*, 2010, **39**, 4206.
12. S. Xiao, M. Shen, R. Guo, S. Wang, X. Shi, *J. Phys. Chem. C*, 2009, **113**, 18062.
13. B. Liu, H. Yang, H. Zhao, L. An, L. Zhang, R. Shi, L. Wang, L. Bao, Y. Chen, *Sens. Actuators, B*, 2011, **156**, 251.
14. P. Wei, W. Hui, L. Dandan, L. Heping, Z. Wei, *Curr. Org. Chem.*, 2013, **17**, 1371.
15. X. Wang, X. Li, X. Sun, F. Li, Q. Liu, Q. Wang, D. He, *J. Mater. Chem.*, 2011, **21**, 3571.
16. Y. Zhang, Y. Wang, J. Jiab, J. Wang, *Sens. Actuators, B*, 2012, **171**, 580.
17. M. Z. Sialvi, R. J. Mortimer, G. D. Wilcox, A. M. Teridi, T. S. Varley, K. G. U. Wijayantha, C. A. Kirk, *ACS Appl. Mater. Interfaces*, 2013, **5**, 5675.
18. R. S. Devan, R. A. Patil, J. H. Lin, Y. R. Ma, *Adv. Funct. Mater.*, 2012, **22**, 3326.
19. D. Li, Y. Wang, Y. Xia, *Nano lett.*, 2003, **3**, 1167.
20. D. Li, Y. Xia, *Adv. Mater.*, 2004, **16**, 1151.
21. I. S. Chronakis, *J. Mater. Process. Technol.*, 2005, **167**, 283.
22. C. D. Saquing, C. Tang, B. C. Monian, A. Bonino, J. L. Manasco, E. Alsborg, S. A. Khan, *Ind. Eng. Chem. Res.*, 2013, **52**, 8692.
23. R. Sahay, P. S. Kumar, R. Sridhar, J. Sundaramurthy, J. Venugopal, S. G. Mhaisalkar, S. Ramakrishna, *J. Mater. Chem.*, 2012, **22**, 12953.
24. X. Xu, L. Jiang, Z. Zhou, X. Wu, Y. Wang, *ACS Appl. Mater. Interfaces*, 2012, **4**, 4331.
25. G. A. M. Hussein, A. K. H. Nohman, K.M.A. Attyia, *J. Therm. Anal.*, 1994, **42**, 1155.
26. Z. He, W. Que, J. Chen, X. Yin, Y. He, J. Ren, *ACS Appl. Mater. Interfaces*, 2012, **4**, 6816.
27. N. Wetchakun, S. Chaiwichain, B. Inceesungvorn, K. Pingmuang, S. Phanichphant, A. I. Minett, J. Chen, *ACS Appl. Mater. Interfaces*, 2012, **4**, 3718.
28. S. G. Kumar, L. G. Devi, *J. Phys. Chem. A*, 2011, **115**, 13211.
29. T. Wu, G. Liu, J. Zhao, H. Hidaka, N. Serpone, *J. Phys. Chem. B*, 1998, **102**, 5845.
30. S. Erdemoğlu, S. K. Aksub, F. Sayilkan, B. İzgi, M. Asiltürk, H. Sayilkan, F. Frimmel, S. Güçer, *J. Hazard. Mater.*, 2008, **155**, 469.
31. M. N. Chong, B. Jin, C. W. K. Chow, C. Saint, *Water Res.*, 2010, **44**, 2997.
32. D. Bahnemann, *Sol. Energy*, 2004, **77**, 445.
33. I. K. Konstantinou, T. A. Albanis, *Appl. Catal., B*, 2004, **49**, 1.
34. L. Wang, A. Wang, *J. Hazard. Mater.*, 2008, **160**, 173.
35. F. Motahari, M. R. Mozdianfar, F. Soofivand, M. S. Niasari, *RSC Adv.*, 2014, DOI: 10.1039/C4RA02697G.
36. K. Ttanaka, K. Padermpole, T. Hisanaga, *Wat. Res.*, 2000, **34**, 327.
37. J. Lei, W. Wang, M. Song, B. Dong, Z. Li, C. Wang, L. Li, *React. Funct. Polym.*, 2011, **71**, 1071.
38. H. Zhua, R. Jianga, L. Xiaob, Y. Changb, Y. Guana, X. Li, G. Zeng, *J. Hazard. Mater.*, 2009, **169**, 933.